Zernike polynomials: a guide

Article *in* Journal of Modern Optics · April 2011

Impact Factor: 1.01 · DOI: 10.1080/09500340.2011.633763

2 authors:

Vasudevan Lakshminarayanan
University of Michigan
323 PUBLICATIONS **1,341** CITATIONS
SEE PROFILE

Andre Fleck
Grand River Hospital
33 PUBLICATIONS **1,007** CITATIONS
SEE PROFILE

Journal of Modern Optics
Vol. 58, No. 7, 10 April 2011, 545–561

Taylor & Francis
Taylor & Francis Group

TUTORIAL REVIEW

Zernike polynomials: a guide

Vasudevan Lakshminarayanan[a,b*†] and Andre Fleck[a,c]

[a]*School of Optometry, University of Waterloo, Waterloo, Ontario, Canada;* [b]*Michigan Center for Theoretical Physics, University of Michigan, Ann Arbor, MI, USA;* [c]*Grand River Hospital, Kitchener, Ontario, Canada*

(*Received 5 October 2010; final version received 9 January 2011*)

In this paper we review a special set of orthonormal functions, namely Zernike polynomials which are widely used in representing the aberrations of optical systems. We give the recurrence relations, relationship to other special functions, as well as scaling and other properties of these important polynomials. Mathematica code for certain operations are given in the Appendix.

Keywords: optical aberrations; Zernike polynomials; special functions; aberrometry

1. Introduction

The Zernike polynomials are a sequence of polynomials that are continuous and orthogonal over a unit circle. A large fraction of optical systems in use today employ imaging elements and pupils which are circular. As a result, Zernike polynomials have been adopted as a mathematical description of optical wavefronts propagating through such systems. An optical wavefront can be thought of as the surface of equivalent phase for radiation produced by a monochromatic light source. For a point source at infinite distance this surface is a plane wave. An example is shown in Figure 1 with an aberrated wavefront for comparison. The mathematical description, offered by Zernike polynomials, is useful in defining the magnitude and characteristics of the differences between the image formed by an optical system and the original object. These optical aberrations can be a result of optical imperfections in the individual elements of an optical system and/or the system as a whole. First employed by F. Zernike, in his phase contrast method for testing circular mirrors [3], they have since gained widespread use due to their orthogonality and their balanced representation of classical aberrations yielding minimum variance over a circular pupil [4–9].

The Zernike polynomials are but one of infinite number of complete sets of polynomials, with two variables, that are orthogonal and continuous over the interior of a unit circle [10]. The condition of being continuous is important to note because, in general, the Zernikes will not be orthogonal over a discrete set of points within a unit circle [11]. However, Zernike polynomials offer distinct advantages over other polynomial sequences. Using the normalized Zernike expansion to describe aberrations offers the advantage that the coefficient or value of each mode represents the root mean square (RMS) wavefront error attributable to that mode. The Zernike coefficients used to mathematically describe a wavefront are independent of the number of polynomials used in the sequence. This condition of independence or orthogonality, means that any number of additional terms can be added without impact on those already computed. Coefficients of larger magnitude indicate greater contribution of that particular mode to the total RMS wavefront error of the system and thus greater negative impact on the optical performance of the system.

Having stated the advantages of Zernike polynomials in describing wavefront aberrations over a unit circle it should also be clearly noted that Zernike polynomials are not always the best polynomials for fitting wavefront test data. In certain cases, Zernike polynomials may provide a poor representation of the wavefront. Some of the effects of air turbulence in astronomy and effects of fabrication errors in the production of optical elements may not be well represented by even a large expansion of the Zernike sequence. In the testing of conical optical elements or irregular ocular optics, such as a condition known as keratoconus (literally a cone shaped cornea),

*Corresponding author. Email: vengu@uwaterloo.ca
†VL is also with the departments of Physics and Electrical Engineering at the University of Waterloo.

ISSN 0950–0340 print/ISSN 1362–3044 online

DOI: 10.1080/09500340.2011.554896
http://www.informaworld.com

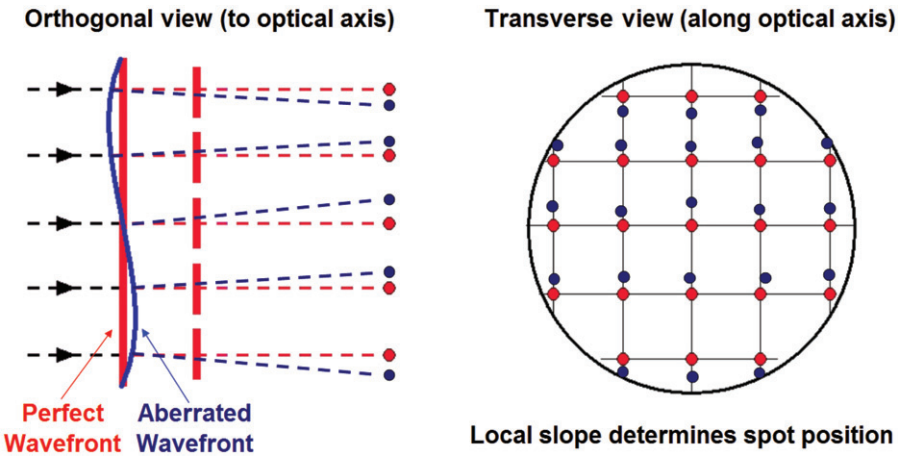

Figure 1. A plane wave (perfect wavefront) and an aberrated wavefront subdivided into smaller wavefronts where the local slope determines the location of a ray tracing projection of the sublet (subdivided wavelet). This is the operating principle of wavefront sensors [1]. (The color version of this figure is included in the online version of the journal.)

additional terms must be added to Zernike polynomials to accurately represent alignment errors and even in so doing, the description of the optical quality may be incomplete [12]. In any system with noncircular pupils, the Zernike circle polynomials will not be orthogonal over the whole of the pupil area and thus may not be the ideal polynomial sequence.

2. Mathematical basis

In general, the function describing an arbitrary wavefront in polar coordinates (r, θ), denoted by $W(r, \theta)$, can be expanded in terms of a sequence of polynomials Z that are orthonormal over the entire surface of the circular pupil:

$$W(r,\theta) = \sum_{n,\,m} C_n^m Z_n^m(r,\theta), \tag{1}$$

where C denotes the Zernike amplitudes or coefficients and Z the polynomials. The coordinate system is shown in Figure 2.

The Zernike polynomials expressed in polar coordinates ($X = r\sin\theta$, $Y = r\cos\theta$) are given by the complex combination:

$$\begin{aligned} Z_n^m(r,\theta) \pm \mathrm{i}Z_n^{-m}(r,\theta) &= V_n^{-m}(r\cos\theta, r\sin\theta) \\ &= R_n^m(r)\exp(\pm \mathrm{i}m\theta), \end{aligned}$$

which leads to

$$\begin{aligned} Z_n^m(r,\theta) &= R_n^m(r)\cos m\theta \quad \text{for } m \geq 0, \\ Z_n^{-m}(r,\theta) &= R_n^m(r)\sin m\theta \quad \text{for } m < 0, \end{aligned} \tag{2}$$

where r is restricted to the unit circle $(0 \leq r \leq 1)$, meaning that the radial coordinate is normalized by the semi-diameter of the pupil, and θ is measured clockwise from the y-axis. This is consistent with aberration theory definitions, but different from the conventional mathematical definition of polar coordinates. The convention employed is at the discretion of the author and may differ depending on the application. The radial function, $R_n^m(r)$, is described by:

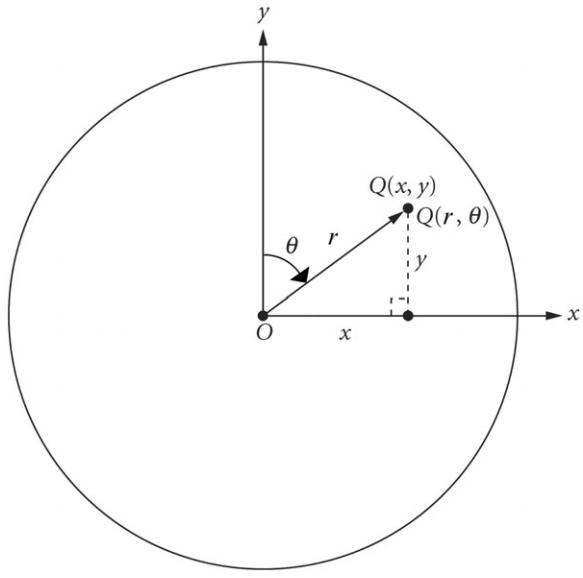

Figure 2. Cartesian (x, y) and polar (r, θ) coordinates of a point Q in the plane of a unit circle representing the circular exit pupil of an imaging system [6].

$$R_n^m(r) = \sum_{l=0}^{(n-m)/2} \frac{(-1)^l (n-l)!}{l!\left[\frac{1}{2}(n+m)-l\right]!\left[\frac{1}{2}(n-m)-l\right]!} r^{n-2l}. \tag{3}$$

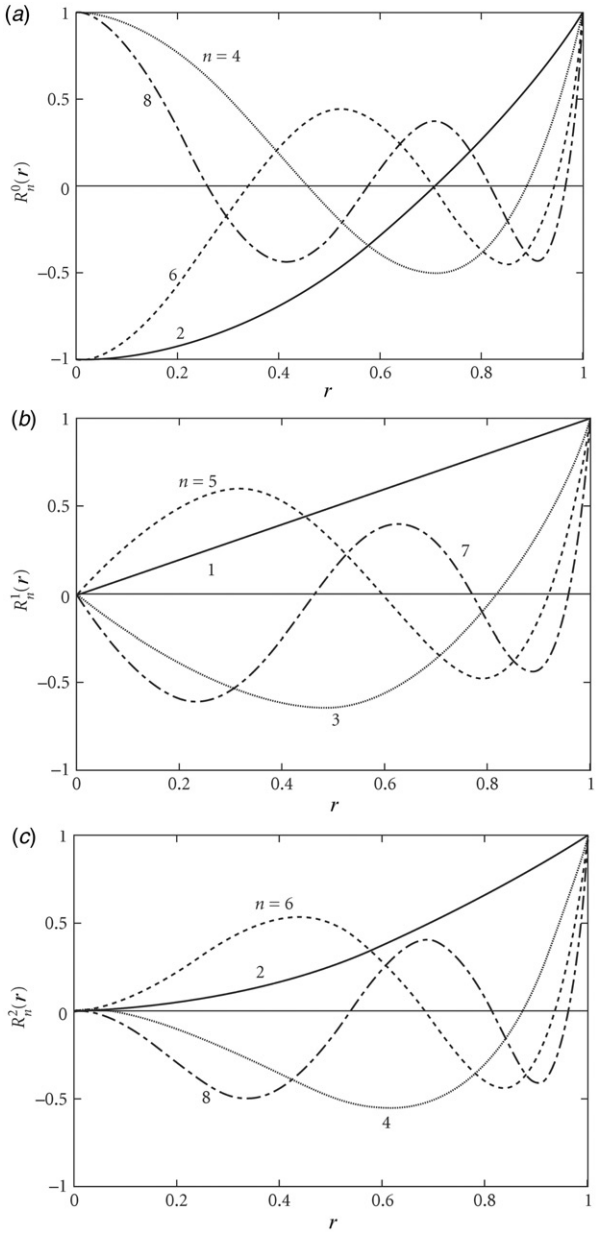

Figure 3. (*a*) The Zernike radial function for $m=0$, $n=2$ (defocus), 4 (spherical aberration), 6, 8 [6]. (*b*) The Zernike radial function for $m=1$, $n=1, 3, 5, 7$. (*c*) The Zernike radial function for $m=2$, $n=2, 4, 6, 8$ [6].

The radial function is plotted in Figure 3 for the first four radial orders for the angular frequency 1, 2 and 3. The first 10 orders of the Zernike polynomial sequence are shown as surface plots in Figure 4. The first three radial orders, $r=0,1,2$ are called low order aberrations and radial orders 3 and above are called higher order aberrations. It should be noted that the radial order 2 is of special interest in visual/ophthalmic optics; it is nothing but the ordinary spectacle correction that is commonly prescribed by optometrists. Furthermore, the radial order $n=1$ is equivalent to prism terms that are prescribed in spectacles as well.

The normalization has been chosen to satisfy $R_n^{\pm m}(1)=1$ for all values of n and m. This gives a normalization constant described by:

$$N_n^m = \left(\frac{2(n+1)}{1+\delta_{m0}}\right)^{1/2}, \tag{4}$$

where δ_{m0} is the Kronecker delta ($\delta_{m0}=0$ for $m\neq 0$).

The algebraic form of the first 10 orders of Zernike polynomials which correspond to the surface plots of Figure 4 are shown in Tables 1 and 2, in both polar and Cartesian form, for comparison. In Cartesian coordinates, the $0\leq r\leq 1$ limit becomes $x^2+y^2\leq 1$, and the recursion relationship for the sequence in Cartesian form is given by [13]:

$$Z_n^m(x,y) = \sum_{i=0}^{q}\sum_{j=0}^{M}\sum_{k=0}^{M-J}(-1)^{i+j}\binom{n-2M}{2i+p}\binom{M-j}{k} \times \frac{(n-j)!}{j!(M-j)!(n-M-j)!}x^{\xi}y^{\eta}, \tag{5}$$

where

$$M=\frac{n}{2}-\left|m-\frac{n}{2}\right|, \quad p=\frac{|s|}{2}(s+1),$$
$$q=(d-s\mathrm{Mod}[n,2])\frac{s}{2}, \quad s=\mathrm{sgn}(d), \quad d=n-2m,$$
$$\xi=2(i+k)+p, \quad \eta=n-2(i+j+k)-p.$$

As can be seen from the relationship above and the expanded form shown in Tables 1 and 2, representation of the polynomials in polar form offers some advantage in efficiency by nature of its circular symmetry. Tables of Zernikes are given, for example, by Born and Wolf [4] and in the article by Noll [9]. However, there is a difference between the two: each of Noll's polynomials should be multiplied by a factor $1/(2(n+1))^{1/2}$ to get the terms given by Born and Wolf.

Although different indexing schemes exist for the Zernike polynomial sequence, the recommended double indexing scheme is portrayed [14,15]. Occasionally a single indexing scheme is used for describing the Zernike expansion coefficients. Since the polynomials depend upon two parameters n and m, ordering of a single indexing scheme is arbitrary. To obtain the single index j, it is convenient to lay out the polynomials in a pyramid with row number n and

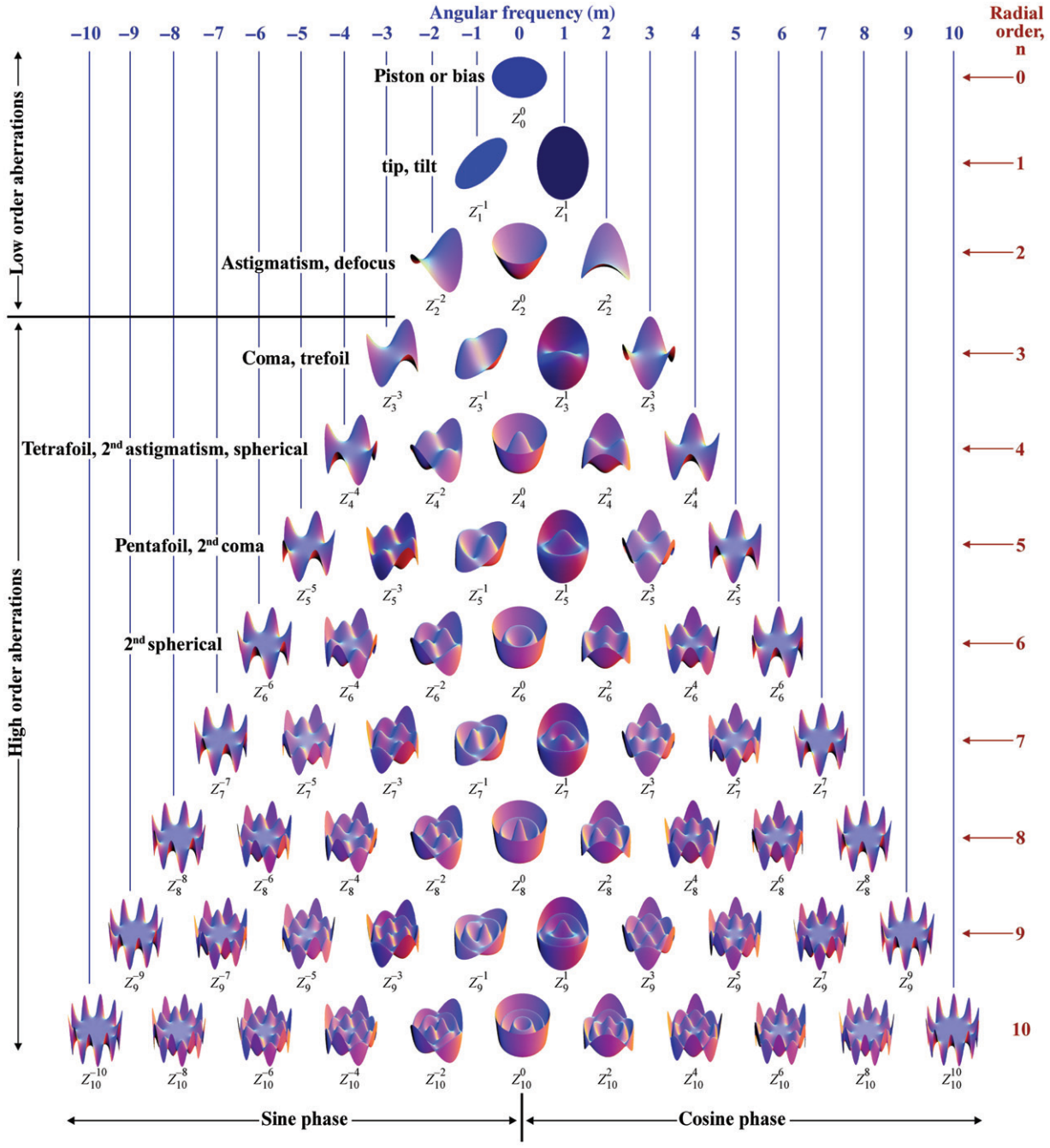

Figure 4. Surface plots of the Zernike polynomial sequence up to 10 orders. The name of the classical aberration associated with some of them is also provided. (The color version of this figure is included in the online version of the journal.)

column number m. The single index, j, starts at the top and the corresponding single indexing scheme, with index variable j, is shown in Table 3.

In the single index scheme:

$$Z_j(r,\theta) = Z_n^m(r,\theta) \tag{6}$$

where $j = [n(n+2)+m]/2$, $n = \text{roundup}\ [(-3+(9+8j)^{1/2})/2]$ and $m = 2j - n(n+2)$.

In this article we will deal exclusively with the double indexed Zernike polynomials. Some older literature does use the single index scheme and because of the variety of indexing schemes that are available

Table 1. Algebraic expansion of the Zernike polynomial sequence, orders one through seven [2].

	n	m	Z_n^m	*RMS*	*Polar form* $(dx^2 \to r\,d\theta\,dr)$	*Cartesian form* $(dx^2 \to dx\,dy)$
	0	0	Z_0^0	$\sqrt{2}$	1	1
	1	−1	Z_1^{-1}	2	$r\sin\theta$	x
	1	1	Z_1^1	2	$r\cos\theta$	y
	2	−2	Z_2^{-2}	$\sqrt{6}$	$r^2\sin 2\theta$	$2xy$
	2	0	Z_2^0	$\sqrt{3}$	$2r^2 - 1$	$-1+2x^2+2y^2$
	2	2	Z_2^2	$\sqrt{6}$	$r^2\cos 2\theta$	$-x^2+y^2$
	3	−3	Z_3^{-3}	$2\sqrt{2}$	$r^3\sin 3\theta$	$-x^3+3xy^2$
	3	−1	Z_3^{-1}	$2\sqrt{2}$	$(3r^3-2r)\sin\theta$	$-2x+3x^3+3xy^2$
	3	1	Z_3^1	$2\sqrt{2}$	$(3r^3-2r)\cos\theta$	$-2y+3y^3+3x^2y$
	3	3	Z_3^3	$2\sqrt{2}$	$r^3\cos 3\theta$	y^3-3x^2y
	4	−4	Z_4^{-4}	$\sqrt{10}$	$r^4\sin 4\theta$	$-4x^3y+4xy^3$
	4	−2	Z_4^{-2}	$\sqrt{10}$	$(4r^4-3r^2)\sin 2\theta$	$-6xy+8x^3y+8xy^3$
	4	0	Z_4^0	$\sqrt{5}$	$6r^4-6r^2+1$	$1-6x^2-6y^2+6x^4+12x^2y^2+6y^4$
	4	2	Z_4^2	$\sqrt{10}$	$(4r^4-3r^2)\cos 2\theta$	$3x^2-3y^2-4x^4+4y^4$
	4	4	Z_4^4	$\sqrt{10}$	$r^4\cos 4\theta$	$x^4-6x^2y^2+y^4$
	5	−5	Z_5^{-5}	$2\sqrt{3}$	$r^5\sin 5\theta$	$x^5-10x^3y^2+5xy^4$
	5	−3	Z_5^{-3}	$2\sqrt{3}$	$(5r^5-4r^3)\sin 3\theta$	$4x^3-12xy^2-5x^5+10x^3y^2+15xy^4$
	5	−1	Z_5^{-1}	$2\sqrt{3}$	$(10r^5-12r^3+3r)\sin\theta$	$3x-12x^3-12xy^2+10x^5+20x^3y^2+10xy^4$
	5	1	Z_5^1	$2\sqrt{3}$	$(10r^5-12r^3+3r)\cos\theta$	$3y-12y^3-12x^2y+10y^5+20x^2y^3+10x^4y$
	5	3	Z_5^3	$2\sqrt{3}$	$(5r^5-4r^3)\cos 3\theta$	$-4y^3+12x^2y+5y^5-10x^2y^3-15x^4y$
	5	5	Z_5^5	$2\sqrt{3}$	$r^5\cos 5\theta$	$y^5-10x^2y^3+5x^4y$
	6	−6	Z_6^{-6}	$\sqrt{14}$	$r^6\sin 6\theta$	$6x^5y-20x^3y^3+6xy^5$
	6	−4	Z_6^{-4}	$\sqrt{14}$	$(6r^6-5r^4)\sin 4\theta$	$20x^3y-20xy^3-24x^5y+24xy^5$
	6	−2	Z_6^{-2}	$\sqrt{14}$	$(15r^6-20r^4+6r^2)\sin 2\theta$	$12xy-40x^3y-40xy^3+30x^5y+60x^3y^3-30xy^5$
	6	0	Z_6^0	$\sqrt{7}$	$20r^6-30r^4+12r^2-1$	$-1+12x^2+12y^2-30x^4-60x^2y^2-30y^4+20x^6+60x^4y^2+60x^2y^4+20y^6$
	6	2	Z_6^2	$\sqrt{14}$	$(15r^6-20r^4+6r^2)\cos 2\theta$	$-6x^2+6y^2+20x^4-20y^4-15x^6-15x^4y^2+15x^2y^4+15y^6$
	6	4	Z_6^4	$\sqrt{14}$	$(6r^6-5r^4)\cos 4\theta$	$-5x^4+30x^2y^2-5y^4+6x^6-30x^4y^2-30x^2y^4+6y^6$
	6	6	Z_6^6	$\sqrt{14}$	$r^6\cos 6\theta$	$-x^6+15x^4y^2-15x^2y^4+y^6$
	7	−7	Z_7^{-7}	4	$r^7\sin 7\theta$	$-x^7+21x^5y^2-35x^3y^4+7xy^6$
	7	−5	Z_7^{-5}	4	$(7r^7-6r^5)\sin 5\theta$	$-6x^5+60x^3y^2-30xy^4+7x^7-63x^5y^2-35x^3y^4+35xy^6$
	7	−3	Z_7^{-3}	4	$(2r^7-30r^5+10r^3)\sin 3\theta$	$-10x^3+30xy^2+30x^5-60x^3y^2-90xy^4-21x^7+21x^5y^2+105x^3y^4+63xy^6$
	7	−1	Z_7^{-1}	4	$(35r^7-60r^5+30r^3-4r)\sin\theta$	$-4x+30x^3+30xy^2-60x^5-120x^3y^2-60xy^4+35x^7+105x^5y^2+105x^3y^4+35xy^6$
	7	1	Z_7^1	4	$(35r^7-60r^5+30r^3-4r)\cos\theta$	$-4y+30y^3+30x^2y-60y^5-120x^2y^3-60x^4y+35y^7+105x^2y^5+105x^4y^3+35x^6y$
	7	3	Z_7^3	4	$(2r^7-30r^5+10r^3)\cos 3\theta$	$10y^3-30x^2y-30y^5+60x^2y^3+90x^4y+21y^7-21x^2y^5-105x^4y^3+63x^6y$
	7	5	Z_7^5	4	$(7r^7-6r^5)\cos 5\theta$	$-6y^5+60x^2y^3-30x^4y+7y^7-63x^2y^5-35x^4y^3+35x^6y$
	7	7	Z_7^7	4	$r^7\cos 7\theta$	$y^7-21x^2y^5+35x^4y^3-7x^6y$

and have been employed in the past, care should be taken when comparing results from different journal articles and software packages.

3. Orthonormality

The orthonormality of the Zernike polynomial sequence is expressed by:

$$\int_0^1\int_0^{2\pi} Z_j(r,\theta)Z_{j'}(r,\theta)r\,\mathrm{d}r\,\mathrm{d}\theta \Big/ \int_0^1\int_0^{2\pi} r\,\mathrm{d}r\,\mathrm{d}\theta = \delta_{jj'}, \quad (7)$$

where $\delta_{jj'} = 1$ if $j = j'$, $\delta_{jj'} = 0$ if $j \neq j'$. This can be separated into its radial orthogonality component given by:

$$\int_0^1 R_n^m(r)R_{n'}^m(r)r\,\mathrm{d}r = \frac{1}{2(n+1)}\delta_{nn'} \quad (8)$$

and angular orthogonality component:

$$\int_0^{2\pi}\mathrm{d}\theta\begin{Bmatrix}\cos m\theta\cos m'\theta\\ \sin m\theta\sin m'\theta\\ \cos m\theta\sin m'\theta\\ \sin m\theta\cos m'\theta\end{Bmatrix} = \begin{Bmatrix}\pi(1+\delta_{m0})\delta_{mm'}\\ \pi\delta_{mm'}\\ 0\\ 0\end{Bmatrix} \quad (9)$$

Table 2. Algebraic expansion of the Zernike polynomial sequence, orders seven through 10 [2].

	n	m	Z_n^m	*RMS*	*Polar form* $(dx^2 \to rd\theta dr)$	*Cartesian form* $(dx^2 \to dxdy)$
	8	–8	Z_8^{-8}	$3\sqrt{2}$	$r^8\sin 8\theta$	$-8x^7y + 56x^5y^3 - 56x^3y^5 + 8xy^7$
	8	–6	Z_8^{-6}	$3\sqrt{2}$	$(8r^8 - 7r^6)\sin 6\theta$	$-42x^5y + 140x^3y^3 - 42xy^5 + 48x^7y - 112x^5y^3 - 112x^3y^5 + 48xy^7$
	8	–4	Z_8^{-4}	$3\sqrt{2}$	$(28r^8 - 42r^6 + 15r^4)\sin 4\theta$	$-60x^3y + 60xy^3 + 168x^5y - 168xy^5 - 112x^7y - 112x^5y^3 + 112x^3y^5 + 112xy^7$
	8	–2	Z_8^{-2}	$3\sqrt{2}$	$(56r^8 - 105r^6 + 60r^4 - 10r^2)\sin 2\theta$	$-20xy + 120x^3y + 120xy^3 - 210x^5y - 420x^3y^3 - 210xy^5 - 112x^7y + 336x^5y^3 + 336x^3y^5 + 112xy^7$
	8	0	Z_8^0	3	$70r^8 - 140r^6 + 90r^4 - 20r^2 + 1$	$1 - 20x^2 - 20y^2 + 90x^4 + 180x^2y^2 + 90y^4 - 140x^6 - 420x^4y^2 - 420x^2y^4 - 140y^6 + 70x^8 + 280x^6y^2 + 420x^4y^4 + 280x^2y^6 + 70y^8$
	8	2	Z_8^2	$3\sqrt{2}$	$(56r^8 - 105r^6 + 60r^4 - 10r^2)\cos 2\theta$	$10x^2 - 10y^2 - 60x^4 + 105x^4y^2 - 105x^2y^4 + 60y^4 + 105x^6 - 105y^6 - 56x^8 - 112x^6y^2 + 112x^2y^6 + 56y^8$
	8	4	Z_8^4	$3\sqrt{2}$	$(28r^8 - 42r^6 + 15r^4)\cos 4\theta$	$15x^4 - 90x^2y^2 + 15y^4 - 42x^6 + 210x^4y^2 + 210x^2y^4 - 42y^6 + 28x^8 - 112x^6y^2 - 280x^4y^4 - 112x^2y^6 + 28y^8$
	8	6	Z_8^6	$3\sqrt{2}$	$(8r^8 - 7r^6)\cos 6\theta$	$7x^6 - 105x^4y^2 + 105x^2y^4 - 7y^6 - 8x^8 + 112x^6y^2 - 112x^2y^6 + 8y^8$
	8	8	Z_8^8	$3\sqrt{2}$	$r^8\cos 8\theta$	$x^8 - 28x^6y^2 + 70x^4y^4 - 28x^2y^6 + y^8$
	9	–9	Z_9^{-9}	$2\sqrt{5}$	$r^9\sin 9\theta$	$x^9 - 36x^7y^2 + 126x^5y^4 - 84x^3y^6 + 9xy^8$
	9	–7	Z_9^{-7}	$2\sqrt{5}$	$(9r^9 - 8r^7)\sin 7\theta$	$8x^7 - 168x^5y^2 + 280x^3y^4 - 56xy^6 - 9x^9 + 180x^7y^2 - 126x^5y^4 - 252x^3y^6 + 63xy^8$
	9	–5	Z_9^{-5}	$2\sqrt{5}$	$(36r^9 - 56r^7 + 21r^5)\sin 5\theta$	$21x^5 - 210x^3y^2 + 105xy^4 - 56x^7 + 504x^5y^2 + 280x^3y^4 - 280xy^6 + 36x^9 - 288x^7y^2 - 504x^5y^4 + 180xy^8$
	9	–3	Z_9^{-3}	$2\sqrt{5}$	$(84r^9 - 168r^7 + 105r^5 - 20r^3)\sin 3\theta$	$20x^3 - 60xy^2 - 105x^5 + 210x^3y^2 + 315xy^4 + 168x^7 - 168x^5y^2 - 840x^3y^4 - 504xy^6 - 84x^9 + 504x^5y^4 + 672x^3y^6 + 252xy^8$
	9	–1	Z_9^{-1}	$2\sqrt{5}$	$(126r^9 - 280r^7 + 210r^5 - 60r^3 + 5r)\sin\theta$	$5x - 60x^3 - 60xy^2 + 210x^5 + 420x^3y^2 + 210xy^4 - 280x^7 - 840x^5y^2 - 840x^3y^4 - 280xy^6 + 126x^9 + 504x^7y^2 + 756x^5y^4 + 504x^3y^6 + 126xy^8$
	9	1	Z_9^1	$2\sqrt{5}$	$(126r^9 - 280r^7 + 210r^5 - 60r^3 + 5r)\cos\theta$	$5y - 60y^3 - 60x^2y + 210y^5 + 420x^2y^3 + 210x^4y - 280y^7 - 840x^2y^5 - 840x^4y^3 - 280x^6y + 126y^9 + 504x^2y^7 + 756x^4y^5 + 504x^6y^3 + 126x^8y$
	9	3	Z_9^3	$2\sqrt{5}$	$(84r^9 - 168r^7 + 105r^5 - 20r^3)\cos 3\theta$	$-20y^3 + 60x^2y + 105y^5 - 210x^2y^3 - 315x^4y - 168y^7 + 168x^2y^5 + 840x^4y^3 + 504x^6y + 84y^9 - 504x^4y^5 - 672x^6y^3 - 252x^8y$
	9	5	Z_9^5	$2\sqrt{5}$	$(36r^9 - 56r^7 + 21r^5)\cos 5\theta$	$21y^5 - 210x^2y^3 + 105x^4y - 56y^7 + 504x^2y^5 + 280x^4y^3 - 280x^6y + 36y^9 - 288x^2y^7 - 504x^4y^5 + 180x^8y$
	9	7	Z_9^7	$2\sqrt{5}$	$(9r^9 - 8r^7)\cos 7\theta$	$-8y^7 + 168x^2y^5 - 280x^4y^3 + 56x^6y + 9y^9 - 180x^2y^7 + 126x^4y^5 + 252x^6y^3 - 63x^8y$
	9	9	Z_9^9	$2\sqrt{5}$	$r^9\cos 9\theta$	$y^9 - 36x^2y^7 + 126x^4y^5 - 84x^6y^3 + 9x^8y$
	10	–10	Z_{10}^{-10}	$\sqrt{22}$	$r^{10}\sin 10\theta$	$10x^9y - 120x^7y^3 + 252x^5y^5 - 120x^3y^7 + 10xy^9$
	10	–8	Z_{10}^{-8}	$\sqrt{22}$	$(10r^{10} - 9r^8)\sin 8\theta$	$72x^7y - 504x^5y^3 + 504x^3y^5 - 72xy^7 - 80x^9y + 480x^7y^3 - 480x^3y^7 + 80xy^9$
	10	–6	Z_{10}^{-6}	$\sqrt{22}$	$(45r^{10} - 72r^8 + 28r^6)\sin 6\theta$	$270x^9y - 360x^7y^3 - 1260x^5y^5 - 360x^3y^7 + 270xy^9 - 432x^7y + 1008x^5y^3 + 1008x^3y^5 - 432xy^7 + 168x^5y - 560x^3y^3 + 168xy^5$
	10	–4	Z_{10}^{-4}	$\sqrt{22}$	$(120r^{10} - 252r^8 + 168r^6 - 35r^4)\sin 4\theta$	$140x^3y - 140xy^3 - 672x^5y + 672xy^5 + 1008x^7y + 1008x^5y^3 - 1008x^3y^5 - 1008xy^7 - 480x^9y - 960x^7y^3 + 960x^3y^7 + 480xy^9$
	10	–2	Z_{10}^{-2}	$\sqrt{22}$	$(210r^{10} - 504r^8 + 420r^6 - 140r^4 + 15r^2)\sin 2\theta$	$30xy - 280x^3y - 280xy^3 + 840x^5y + 1680x^3y^3 + 840xy^5 - 1008x^7y - 3024x^5y^3 - 3024x^3y^5 - 1008xy^7 + 420x^9y + 1680x^7y^3 + 2520x^5y^5 + 1680x^3y^7 + 420xy^9$
	10	0	Z_{10}^0	$\sqrt{11}$	$252r^{10} - 630r^8 + 560r^6 - 210r^4 + 30r^2 - 1$	$-1 + 30x^2 + 30y^2 - 210x^4 - 420x^2y^2 - 210y^4 + 560x^6 + 1680x^4y^2 + 1680x^2y^4 + 560y^6 - 630x^8 - 2520x^6y^2 - 3780x^4y^4 - 2520x^2y^6 - 630y^8 + 252x^{10} + 1260x^8y^2 + 2520x^6y^4 + 2520x^4y^6 + 1260x^2y^8 + 252y^{10}$
	10	2	Z_{10}^2	$\sqrt{22}$	$(210r^{10} - 504r^8 + 420r^6 - 140r^4 + 15r^2)\cos 2\theta$	$-15x^2 + 15y^2 + 140x^4 - 140y^4 - 420x^6 - 420x^4y^2 + 420x^2y^4 + 420y^6 + 504x^8 + 1008x^6y^2 - 1008x^2y^6 - 504y^8 - 210x^{10} - 630x^8y^2 - 420x^6y^4 + 420x^4y^6 + 630x^2y^8 + 210y^{10}$
	10	4	Z_{10}^4	$\sqrt{22}$	$(120r^{10} - 252r^8 + 168r^6 - 35r^4)\cos 4\theta$	$-35x^4 + 210x^2y^2 - 35y^4 + 168x^6 - 840x^4y^2 - 840x^2y^4 + 168y^6 - 252x^8 + 1008x^6y^2 + 2520x^4y^4 + 1008x^2y^6 - 252y^8 + 120x^{10} - 360x^8y^2 - 1680x^6y^4 - 1680x^4y^6 - 360x^2y^8 + 120y^{10}$
	10	6	Z_{10}^6	$\sqrt{22}$	$(45r^{10} - 72r^8 + 28r^6)\cos 6\theta$	$-28x^6 + 420x^4y^2 - 420x^2y^4 + 28y^6 + 72x^8 - 1008x^6y^2 + 1008x^2y^6 - 72y^8 - 45x^{10} + 585x^8y^2 + 630x^6y^4 - 630x^4y^6 - 585x^2y^8 + 45y^{10}$
	10	8	Z_{10}^8	$\sqrt{22}$	$(10r^{10} - 9r^8)\cos 8\theta$	$-9x^8 + 252x^6y^2 - 630x^4y^4 + 252x^2y^6 - 9y^8 + 10x^{10} - 270x^8y^2 + 420x^6y^4 + 420x^4y^6 - 270x^2y^8 + 10y^{10}$
	10	10	Z_{10}^{10}	$\sqrt{22}$	$r^{10}\cos 10\theta$	$-x^{10} + 45x^8y^2 - 210x^6y^4 + 210x^4y^6 - 45x^2y^8 + y^{10}$

Table 3. Relationship between single and double index schemes to third order.

Radial order, n	Angular frequency, m						
	-3	-2	-1	0	1	2	3
0				j=0			
1			j=1		j=2		
2		j=3		j=4		j=5	
3	j=6		j=7		j=8		j=9

The sign of the angular frequency, m, determines the angular parity. The polynomial is said to be even when $m \geq 0$ and odd when $m < 0$.

4. Recurrence relations

The relationship between different Zernike modes is given by the following recurrence relations:

$$R_n^m(r) = \frac{1}{2(n+1)r}\left[(n+m+2)R_{n+1}^{m+1}(r) + (n-m)R_{n-1}^{m+1}(r)\right], \tag{10}$$

$$R_{n+2}^m(r) = \frac{n+2}{(n+2)^2 - m^2} \times \left\{\left[4(n+1)r^2 - \frac{(n+m)^2}{n} - \frac{(n-m+2)^2}{n+2}\right] \times R_n^m(r) - \frac{n^2-m^2}{n} R_{n-2}^m(r)\right\}, \tag{11}$$

$$R_n^m(r) + R_n^{m+2}(r) = \frac{1}{n+1}\frac{\mathrm{d}[R_{n+1}^{m+1}(r) - R_{n-1}^{m+1}(r)]}{\mathrm{d}r}. \tag{12}$$

The recurrence procedure can be started using $R_m^m(r) = r^m$. Ideally, a recurrence procedure should be numerically stable and free of errors which propagate and are magnified as the recurrence proceeds [16,17]. For the Zernike recurrence relation above it is found that the recurrence procedure is not absolutely stable in all cases and that, as m increases, small errors in high order terms ($m \sim > 10$) can become magnified. Forbes [18] has shown how to dramatically improve numerical stability of the Zernike expansion to high order.

5. Relationship to other polynomial sequences

The relationship between the Zernike polynomials and other polynomial sequences can be derived. Of particular importance is the formulation with respect to the Bessel function, J,

$$\int_0^1 R_n^m(r) J_m(xr) r\,\mathrm{d}r = (-1)^{(n-m)/2}\frac{J_{n+1}(x)}{x}, \quad \text{where } J_m(x) = \sum_{l=0}^{\infty}\frac{(-1)^l}{2^{2l+m}l!(m+1)!}x^{2l+m}, \tag{13}$$

which has applications in the Nijboer–Zernike theory of diffraction and aberrations [7]. The relationship between Zernike and Jacobi polynomials, P, is given by [2, 4]:

$$R_n^m(r) = (-1)^{(n-m)/2} r^m P_{(n-m)/2}^{(m,0)}(1-r^2), \tag{14}$$

where

$$P_n^{(\alpha,\beta)} = \frac{1}{2}\sum_{m=0}^{n}\binom{n+\alpha}{m}\binom{n+\beta}{n-m}(x-1)^n(x+1)^m \tag{15}$$

between Zernike and the hypergeometric function, F, through:

$$R_n^m(r) = (-1)^{\frac{n-m}{2}}\binom{\frac{1}{2}(n+m)}{m} r^m\, {}_2F_1\left(\frac{n+m+2}{2}, -\frac{n-m}{2}, m+1, r^2\right), \tag{16}$$

where

$${}_2F_1(a,b;c;x) \equiv \sum_{n=0}^{\infty}\frac{(a)_n(b)_n}{(c)_n}\frac{x^n}{n!} \tag{17}$$

and, between Zernike and the Legendre polynomials, P, through:

$$P_n(r) = 2^{-n}\sum_{i=0}^{n/2}(-1)^i\binom{n}{i}\binom{2n-2i}{n} r^{n-2i}, \tag{18}$$

where n is even.

The aberration of a general optical system with a point object can also be represented by a wave aberration polynomial of the form:

$$W(X,Y) = W_1 + W_2X + W_3Y + W_4X^2 + W_5XY + W_6Y^2 + W_7X^3 + W_8X^2Y + W_9XY^2 + W_{10}Y^3 + W_{11}X^4 + W_{12}X^3Y + \cdots; \tag{19}$$

here X and Y are co-ordinates in the entrance pupil. This Taylor series can be represented very simply as:

$$W(X,Y) = \sum_{n=0}^{n=k}\sum_{m=0}^{m=n} W_{\frac{n(n+1)}{2}+m+1}\cdot X^{n-m}Y^m. \tag{20}$$

Table 4. Functions generated from Gram–Schmidt orthogonalization of a power series [2].

Functions	Series	Interval	Weight	Norm
Legendre	$\{1, r, r^2, r^3, \ldots\}$	$-1 \le r \le 1$	1	$2/(2n+1)$
Shifted Legendre	$''$	$0 \le r \le 1$	1	$1/(2n+1)$
Chebyshev I	$''$	$-1 \le r \le 1$	$(1-x^2)^{-1/2}$	$\pi/(2-\delta_0^n)$
Shifted Chebyshev I	$''$	$0 \le r \le 1$	$[x(1-x^2)]^{-1/2}$	$\pi/(2-\delta_0^n)$
Chebyshev II	$''$	$-1 \le r \le 1$	$(1-x^2)^{-1/2}$	$\pi/2$
Associated Laguerre	$''$	$0 \le r < \infty$	$r^k e^{-r}$	$(n+k)!/n!$
Hermite	$''$	$-\infty < r < \infty$	e^{-r2}	$2^n \pi^{1/2} n!$
Zernike radial	$\{r^m, r^{m+2}, r^{m+4}, \ldots\}$	$0 \le r \le 1$	r	$1/(2n+2)$

Any Zernike term can be expressed as a combination of Taylor terms and vice versa. Malacara, for example, provides the matrix transformation relations for conversions up to the 45th term [19].

The Zernike coefficients represent combinations of primary (Seidel) and higher-order aberrations through the expression [20,21]:

$$C_{nm} = \sum_{l=n} \sum_{k=0} T_{nmkl} S_{kl}, \tag{21}$$

where $l - m$ is even,

$$T_{nmkl} = \frac{(n+s)! 2^{2-l}}{(1+\delta_{m0})(\frac{l+m}{2})!(\frac{l-m}{2})!} \times \sum_{s=0}^{(n-m)/2} \frac{(-1)^s (n-s)!}{s!(\frac{n+m}{2}-s)!(\frac{n-m}{2}-s)!(n-2s+k+2)} \tag{22}$$

and $n - m$ must be even as well.

In addition, the other special functions can be generated by performing a Gram–Schmidt orthogonalization of a power series (see [2]; Table 4).

6. Wavefront error

A common metric of wavefront flatness for the wavefront, $W(r,\theta)$, defined in Equation (1) is the RMS wavefront error, σ, or wavefront variance, σ^2,

$$\sigma = \mathrm{RMS_w} = \left(\frac{1}{A} \int_{\text{pupil}} (W(x,y) - \overline{W})^2 \, \mathrm{d}x \, \mathrm{d}y \right)^{1/2}, \tag{23a}$$

where A is the pupil area and $\overline{W}$ is the mean wavefront optical path difference.

The wavefront error or variance can also be computed from a vector of the Zernike amplitudes using:

$$\sigma = \left(\sum_{j=3}^{N} C_j^2 \right)^{1/2}, \tag{23b}$$

where the first few terms representing the pseudo-aberrations of piston, tip and tilt are ignored.

7. Transformations of Zernike coefficients

The mathematical basis by which Zernike coefficients can be transformed analytically with regard to concentric scaling, rotating and translating both circular and elliptical pupils has been developed by several groups [22–27]. Using the matrix method, the wavefront can be expressed as an inner product of $\langle Z|$, a row vector with the Zernike polynomials:

$$\langle Z| = \left| Z_{n_{\max}}^{-n_{\max}} \; Z_{n_{\max}-1}^{-(n_{\max}-1)} \; Z_{n_{\max}-2}^{-(n_{\max}-2)} \; Z_{n_{\max}}^{-(n_{\max}-2)} \; \cdots \; Z_{n_{\max}}^{n_{\max}-2} \times Z_{n_{\max}-1}^{n_{\max}-1} \; Z_{n_{\max}}^{n_{\max}} \right| \tag{24}$$

and $|C\rangle$, a column vector with the corresponding Zernike coefficients:

$$|C\rangle = \begin{vmatrix} C_{n_{\max}}^{-n_{\max}} \\ C_{n_{\max}-1}^{-(n_{\max}-1)} \\ C_{n_{\max}-2}^{-(n_{\max}-2)} \\ C_{n_{\max}}^{-(n_{\max}-2)} \\ \vdots \\ C_{n_{\max}}^{n_{\max}-2} \\ C_{n_{\max}-1}^{n_{\max}-1} \\ C_{n_{\max}}^{n_{\max}} \end{vmatrix} \tag{25}$$

with a form comparable to Equation (1):

$$W(\rho,\theta) = \sum_n \sum_m c_n^m Z_n^m(\rho,\theta) = \langle Z|c\rangle, \tag{26}$$

where $0 \ge (\rho = r/r_0) \ge 1$. In this formalism the Zernike polynomials can be written as:

$$\langle Z| = \langle \rho \, M| \, [\eta] \, [R] \, [N], \tag{27}$$

where

$$\langle \rho M| = \left[\rho^{n_{\max}} \mathrm{e}^{-\mathrm{i}n_{\max}\theta} \; \rho^{n_{\max}} \; -1\mathrm{e}^{-\mathrm{i}(n_{\max}-1)\theta} \; \rho^{n_{\max}} \; -2\mathrm{e}^{-\mathrm{i}(n_{\max}-2)\theta} \; \rho^{n_{\max}} \mathrm{e}^{-\mathrm{i}(n_{\max}-2)\theta} \; \cdots \; \rho^{n_{\max}} \mathrm{e}^{\mathrm{i}n_{\max}\theta} \right], \tag{28}$$

$$[R]=\begin{bmatrix} R_{n_{\max}}^{-n_{\max}} & 0 & 0 & 0 & \cdots & 0 \\ 0 & R_{n_{\max}-1}^{-(n_{\max}-1)} & 0 & 0 & \cdots & 0 \\ 0 & 0 & R_{n_{\max}-2}^{-(n_{\max}-2)} & 0 & \cdots & 0 \\ 0 & 0 & 0 & R_{n_{\max}}^{-(n_{\max}-2)} & \cdots & 0 \\ \vdots & \vdots & \vdots & \vdots & \ddots & \vdots \\ 0 & 0 & 0 & 0 & \cdots & R_{n_{\max}}^{n_{\max}} \end{bmatrix}, \tag{29}$$

$$[N]=\begin{bmatrix} R_{n_{\max}} & 0 & 0 & 0 & \cdots & 0 \\ 0 & R_{n_{\max}-1} & 0 & 0 & \cdots & 0 \\ 0 & 0 & R_{n_{\max}-2} & 0 & \cdots & 0 \\ 0 & 0 & 0 & R_{n_{\max}} & \cdots & 0 \\ \vdots & \vdots & \vdots & \vdots & \ddots & \vdots \\ 0 & 0 & 0 & 0 & \cdots & R_{n_{\max}} \end{bmatrix} \tag{30}$$

and $[\eta]$ is the transformation matrix specific to the type of transformation being considered. The conversion matrix, $[C]$, which yields the new set of Zernike coefficients in terms of the original set is then given by [28]:

$$[C]=[N]^{-1}[R]^{-1}[\eta][R][N]. \tag{31}$$

7.1. Scaled pupil (see Figure 5(a))

For a change in the size of wavefront from r_0 to r_s as depicted in Figure 5(a), the angular coordinate remains unchanged with $\theta=\theta'$ but the radial coordinate is scaled by factor $\eta_s=r_s/r_0$ giving $\rho=\eta_s\rho'$ and:

$$\rho\exp(\mathrm{i}\theta)=\eta_s\rho'\exp(\mathrm{i}\theta'). \tag{32}$$

This, in turn, changes the terms of $\langle\rho M|$ by:

$$\rho^n\exp(\mathrm{i}m\theta)=\eta_s^n\rho'^n\exp(\mathrm{i}m\theta'), \tag{33}$$

where η_s is a diagonal matrix with elements η_s^n. An example of this scaling matrix to third order is shown below [27]:

$$[\eta]_s=\begin{bmatrix} \eta_s^3 & 0 & 0 & 0 & 0 & 0 & 0 & 0 & 0 & 0 \\ 0 & \eta_s^2 & 0 & 0 & 0 & 0 & 0 & 0 & 0 & 0 \\ 0 & 0 & \eta_s & 0 & 0 & 0 & 0 & 0 & 0 & 0 \\ 0 & 0 & 0 & \eta_s^3 & 0 & 0 & 0 & 0 & 0 & 0 \\ 0 & 0 & 0 & 0 & 1 & 0 & 0 & 0 & 0 & 0 \\ 0 & 0 & 0 & 0 & 0 & \eta_s^2 & 0 & 0 & 0 & 0 \\ 0 & 0 & 0 & 0 & 0 & 0 & \eta_s & 0 & 0 & 0 \\ 0 & 0 & 0 & 0 & 0 & 0 & 0 & \eta_s^3 & 0 & 0 \\ 0 & 0 & 0 & 0 & 0 & 0 & 0 & 0 & \eta_s^2 & 0 \\ 0 & 0 & 0 & 0 & 0 & 0 & 0 & 0 & 0 & \eta_s^3 \end{bmatrix}. \tag{34}$$

7.2. Translated pupil (see Figure 5(b))

For a translation of this scaled wavefront by r_t at angle θ_t, as depicted in Figure 5(b), the translation transformation is described by factor $\eta_t=r_t/r_0$ which gives:

$$\rho\exp(\mathrm{i}\theta)=\eta_s\rho'\exp(\mathrm{i}\theta')+\eta_t\exp(\mathrm{i}\theta_t), \tag{35}$$

and after expansion and use of the binomial theorem:

$$\begin{aligned}\rho\exp(\mathrm{i}m\theta)=&\frac{1}{2^n}\sum_{p=0}^{(n+m)/2}\sum_{q=0}^{(n-m)/2}\binom{\frac{n+m}{2}}{p}\binom{\frac{n-m}{2}}{q}\\ &\times(\eta_e+1)^{n-p-q}(n_e-1)^{p+q}\\ &\times\exp[\mathrm{i}2(p-q)\theta_e]\rho'^n\exp[\mathrm{i}(m-2p+2q)\theta'].\end{aligned} \tag{36}$$

An example of this translation and scaling transformation matrix to third order is shown below [27]:

$$[\eta]_t=\begin{bmatrix} \eta_s^3 & 0 & 0 & 0 & 0 & 0 & 0 & 0 & 0 & 0 \\ 3\eta_s^2\eta_t\mathrm{e}^{-\mathrm{i}\theta_t} & \eta_s^2 & 0 & \eta_s^2\eta_t\mathrm{e}^{\mathrm{i}\theta_t} & 0 & 0 & 0 & 0 & 0 & \\ 3\eta_s\eta_t^2\mathrm{e}^{-\mathrm{i}2\theta_t} & 2\eta_s\eta_t\mathrm{e}^{-\mathrm{i}\theta_t} & \eta_s & 2\eta_s\eta_t^2 & 0 & \eta_s\eta_t\mathrm{e}^{\mathrm{i}\theta_t} & 0 & \eta_s\eta_t^2\mathrm{e}^{\mathrm{i}2\theta_t} & 0 & 0 \\ 0 & 0 & 0 & \eta_s^3 & 0 & 0 & 0 & 0 & 0 & 0 \\ \eta_t^3\mathrm{e}^{-3\mathrm{i}\theta_t} & \eta_t^2\mathrm{e}^{-2\mathrm{i}\theta_t} & \eta_t\mathrm{e}^{-\mathrm{i}\theta_t} & \eta_t^3\mathrm{e}^{-\mathrm{i}\theta_t} & 1 & \eta_t^2 & \eta_t\mathrm{e}^{\mathrm{i}\theta_t} & \eta_t^3\mathrm{e}^{\mathrm{i}\theta_t} & \eta_t^2\mathrm{e}^{\mathrm{i}2\theta_t} & \eta_t^3\mathrm{e}^{\mathrm{i}3\theta_t} \\ 0 & 0 & 0 & 2\eta_s^2\eta_t\mathrm{e}^{-\mathrm{i}\theta_t} & 0 & \eta_s^2 & 0 & 2\eta_s^2\eta_t\mathrm{e}^{\mathrm{i}\theta_t} & 0 & 0 \\ 0 & 0 & 0 & \eta_s\eta_t^2\mathrm{e}^{-2\mathrm{i}\theta_t} & 0 & \eta_s\eta_t\mathrm{e}^{-\mathrm{i}\theta_t} & \eta_s & 2\eta_s\eta_t^2 & 2\eta_s\eta_t\mathrm{e}^{\mathrm{i}\theta_t} & 3\eta_s\eta_t^2\mathrm{e}^{\mathrm{i}2\theta_t} \\ 0 & 0 & 0 & 0 & 0 & 0 & 0 & \eta_s^3 & 0 & 0 \\ 0 & 0 & 0 & 0 & 0 & 0 & 0 & \eta_s^2\eta_t\mathrm{e}^{-\mathrm{i}\theta_t} & \eta_s^2 & 3\eta_s^2\eta_t\mathrm{e}^{\mathrm{i}\theta_t} \\ 0 & 0 & 0 & 0 & 0 & 0 & 0 & 0 & 0 & \eta_s^3 \end{bmatrix}. \tag{37}$$

7.3. Rotated pupil (see Figure 5(c))

A rotation by θ_r, as depicted in Figure 5(c), gives:

$$\rho^n\exp(\mathrm{i}m\theta)=\exp(\mathrm{i}m\theta_r)\rho'^n\exp(\mathrm{i}m\theta'), \tag{38}$$

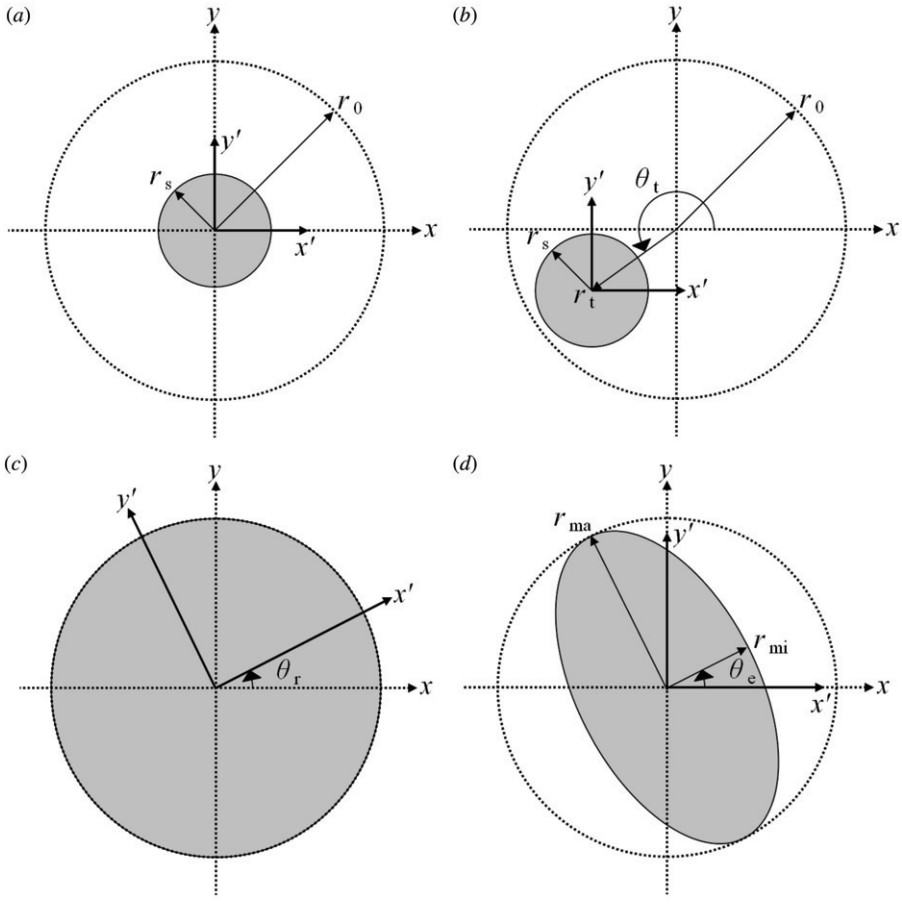

Figure 5. Transformation types: (*a*) scaling of a circular pupil from r_0 to r_s. (*b*) Translation of circular pupil a distance r_t at angle θ_t. (*c*) Rotation of a circular pupil at angle θ_r. (*d*) Transformation for elliptical pupil with major radius r_{ma}, minor radius r_{mi} and rotation angle θ_e.

with rotation transformation matrix example, to third order, shown below:

$$[\eta]_r = \begin{bmatrix} e^{-i3\theta_r} & 0 & 0 & 0 & 0 & 0 & 0 & 0 & 0 & 0 \\ 0 & e^{-i2\theta_r} & 0 & 0 & 0 & 0 & 0 & 0 & 0 & 0 \\ 0 & 0 & e^{-i\theta_r} & 0 & 0 & 0 & 0 & 0 & 0 & 0 \\ 0 & 0 & 0 & e^{-i\theta_r} & 0 & 0 & 0 & 0 & 0 & 0 \\ 0 & 0 & 0 & 0 & 1 & 0 & 0 & 0 & 0 & 0 \\ 0 & 0 & 0 & 0 & 0 & 1 & 0 & 0 & 0 & 0 \\ 0 & 0 & 0 & 0 & 0 & 0 & e^{i\theta_r} & 0 & 0 & 0 \\ 0 & 0 & 0 & 0 & 0 & 0 & 0 & e^{i\theta_r} & 0 & 0 \\ 0 & 0 & 0 & 0 & 0 & 0 & 0 & 0 & e^{i2\theta_r} & 0 \\ 0 & 0 & 0 & 0 & 0 & 0 & 0 & 0 & 0 & e^{i3\theta_r} \end{bmatrix}. \tag{39}$$

7.4. Elliptical pupil (see Figure 5(d))

As stated earlier, the Zernike polynomials are continuous and orthogonal over a unit circle. When a wavefront is measured off axis or with a pupil rotated with respect to an axis orthogonal to the optical axis of the system, the pupil projected onto a flat surface (sensor) will be elliptical. In this case, the Zernike polynomials and coefficients will describe a wavefront extrapolated to areas for which there is no information. The solution adopted [27,28] is to mathematically stretch the elliptical wavefront into a circle, thus correcting for the extrapolation. For the elliptical pupil, shown in Figure 5(*d*), this gives:

$$\begin{aligned} \rho^n \exp(im\theta) = \frac{1}{2^n} \sum_{p=0}^{(n+m)/2} \sum_{q=0}^{(n-m)/2} & \binom{\frac{n+m}{2}}{p} \binom{\frac{n-m}{2}}{q} \\ & \times (\eta_e + 1)^{n-p-q} (\eta_e - 1)^{p+q} \\ & \times \exp[i2(p-q)\theta_e] \rho'^n \exp[i(m-2p+2q)\theta']. \end{aligned} \tag{40}$$

A measurement of a model eye showing the impact on the Zernike coefficients of using both a circular pupil and elliptical pupil is shown in Figure 6 [29]. In this

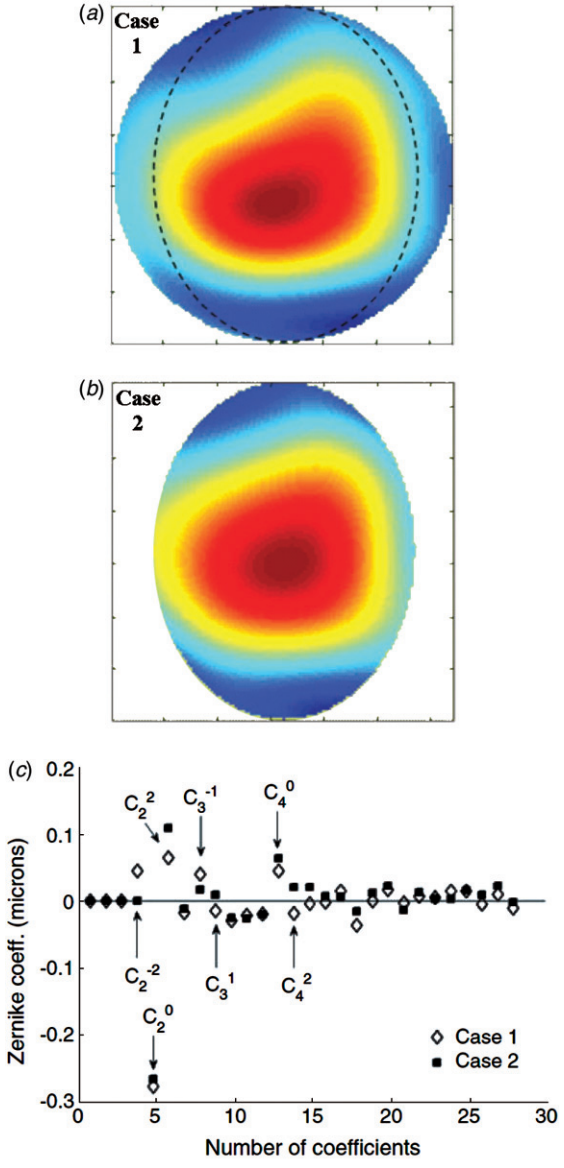

Figure 6. (*a*) A measurement of an aberrated wavefront with a circular pupil and an elliptical pupil overlayed by the dashed line. (*b*) The measured wavefront from the elliptical aperture. (*c*) The change in the first 28 Zernike coefficients (up to six orders) as a result of the change in pupil shape [27]. (The color version of this figure is included in the online version of the journal.)

example, the wavefront is measured with a circular entrance pupil and an elliptical entrance pupil produced by rotating the circular aperture 40°. The long axis of the ellipse is equal to the diameter of the circular pupil. As expected, the change in pupil shape does not impact the defocus term, whereas the unexpected discrepancies for primary astigmatism, vertical coma and secondary astigmatism are thought to be a result of some small, residual misalignment.

8. Primary aberrations

As noted earlier, the primary aberrations of ocular prescriptions, (usually written as Sphere combined with a cylindrical power and specifying the axis of the cylinder) through a pupil of radius, r_0, can be computed from the Zernike amplitudes using:

$$cyl = 2(J_0^2 + J_{45}^2)^{1/2}, \quad sphere = M - \frac{cyl}{2},$$
$$axis = -\arctan\left(\frac{cyl/2 + J_0}{J_{45}}\right), \tag{41}$$

where:

$$M = \frac{-4(3^{1/2})}{r_0^2} C_2^0, \quad J_0 = \frac{-2(6^{1/2})}{r_0^2} C_2^2,$$
$$J_{45} = \frac{-2(6^{1/2})}{r_0^2} C_2^{-2}.$$

9. Zernike polynomials using Fourier transform

For large values of the radial order n, the conventional representation of the radial function of the Zernike polynomials given in Equation (3) can produce unacceptable numerical results. In order to deal with this a possible solution is to convert the Zernike coefficients to a Fourier representation and do a numerical FFT computation [30–32].

The wavefront can be expressed as:

$$W(r,\theta) = \sum_{j=0}^{N^2-1} a_j(k,\varphi) \exp\left(\frac{2\pi \mathrm{i}}{N} \boldsymbol{k} \cdot \boldsymbol{r}\right), \tag{42}$$

where $\boldsymbol{k}$ and $\boldsymbol{r}$ are the position vectors in polar coordinates in the spatial and the frequency domains, respectively, and N^2 is the total number of wavefront sampling points. The relationship between Zernike coefficients and Fourier coefficients is then given by:

$$c_j = \frac{1}{\pi} \sum_{l=0}^{N^2-1} a_l(k,\varphi) U_j^*(k,\varphi), \tag{43}$$

where U_j is the Fourier transform of the Zernike polynomials and given by:

$$U_j(k,\varphi) = \iint P(r) Z_j(r,\theta) \exp(-2\pi \mathrm{i} \boldsymbol{k} \cdot \boldsymbol{r})\, \mathrm{d}\boldsymbol{r}$$
$$= (-1)^{n/2+|m|}(n+1)^{1/2} \frac{J_{n+1}(2\pi k)}{k} \times \begin{cases} 2^{1/2}\cos|m|\theta & (m>0) \\ 1 & (m=0) \\ 2^{1/2}\sin|m|\theta & (m<0) \end{cases} \tag{44}$$

and J_n is the nth-order Bessel function of the first kind.

Fourier full reconstruction has been demonstrated to be more accurate than Zernike reconstruction from sixth to tenth order for random wavefront images with low to moderate noise levels [33]. However, experimentally, Zernike-based reconstruction algorithms have been found to outperform Fourier wavefront reconstruction to fifth order, in terms of the residual RMS error [34]. See [13] regarding numerical stability.

10. Zernike annular polynomials

For a unit annulus with obscuration ratio ϵ, shown in Figure 7(*a*), the wavefunction in Equation (1) can be expanded in terms of this additional variable [35]:

$$W(r,\theta;\epsilon)=\sum_{n,m} C_n^m Z_n^m(r,\theta;\epsilon), \tag{45}$$

where $\epsilon \le r \le 1$ and $0 \le \theta \le 2\pi$. The orthogonality condition of the radial polynomial sequence for an annulus is then given by:

$$\int_{\epsilon}^{1} R_n^m(r;\epsilon)R_{n'}^m(r;\epsilon)r\,\mathrm{d}r=\frac{1-\epsilon^2}{2(n+1)}\delta_{nn'}. \tag{46}$$

The annular polynomials, obtained from the circle polynomials using the Gram–Schmidt orthogonalization process, differ only in their normalization and that they are orthogonal over an annulus, not a circle. Comparing the $m=0$, angularly independent, radial functions for circular and annular Zernike polynomials (Figure 7(*b*) and (*c*)) clearly shows the similarities and radial extent.

11. Gram–Schmidt orthogonalization for apertures of arbitrary shape

An aperture of arbitrary shape can have an orthonormal basis set that is generated from the circular Zernike polynomials apodized by a mask using the Gram–Schmidt orthogonalization technique [20,36]. In general, orthogonality is defined with respect to the inner product:

$$\langle f,g\rangle=\frac{\int \mathrm{d}\boldsymbol{r}\, f(\boldsymbol{r})\, g(\boldsymbol{r})\, H(\boldsymbol{r})}{\int \mathrm{d}\boldsymbol{r}\, H(\boldsymbol{r})}, \tag{47}$$

where H is a zero-one valued function that defines the aperture. For a basis of arbitrary shape defined by the vectors $\{V_1 \ldots V_n\}$, Gram–Schmidt orthogonalization is represented by:

$$V'_n=Z_n+\sum_{m=1}^{n-1} D'_{nm}V_m, \tag{48}$$

where $\{V'_1 \ldots V'_n\}$ are the set of orthonogonal but not orthonormal vectors of the arbitrary shape (hence $V_n=V'_n/||V'_n||$) and $\{Z_1 \ldots Z_n\}$ is the circular Zernike basis. For an orthogonal basis set, D'_{nm} can be calculated and shown to be given by:

$$D'_{nm}=-\langle Z_n,V_m\rangle \tag{49}$$

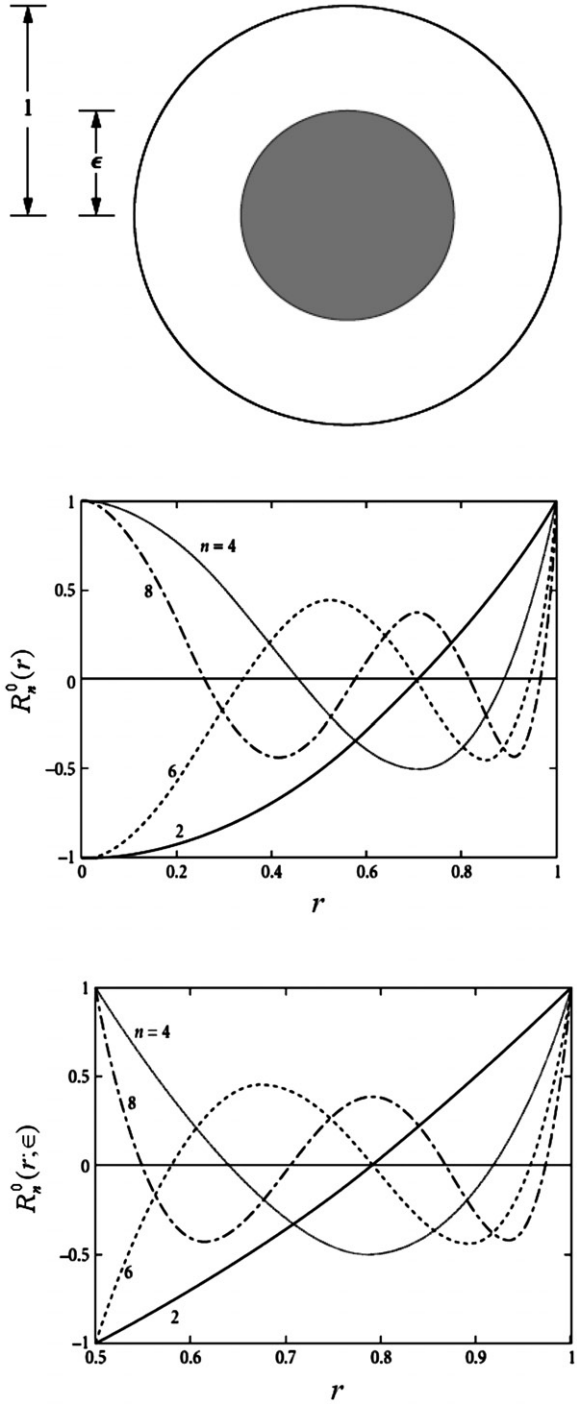

Figure 7. (*a*) Diagram of annular pupil. (*b*) The Zernike circle radial polynomial for $m=0$, $n=2$, 4, 6, 8. (*c*) The Zernike annular radial polynomial with $\epsilon=0.5$, $m=0$, $n=2$, 4, 6, 8 [6].

for each $m < n$. Expressing the new basis $\{V_1 \ldots V_n\}$ in terms of the circular Zernike polynomials then gives:

$$V_i = \sum_{m=1}^{n} C_{im} Z_m, \tag{50}$$

where C is the transformation matrix.

12. Conclusions

The Zernike polynomials are very well suited for mathematically describing wavefronts or the optical path differences of systems with circular pupils. The Zernike polynomials form a complete basis set of functions that are orthogonal over a circle of unit radius. In this paper, the most important properties of the Zernike polynomials have been reviewed including the generating functions of the Zernike polynomials, relationships to other polynomial sets, the orthonormality conditions as well as transformations. It is meant to constitute a reasonable introduction into this exceptionally useful polynomial set with figures that have been combined from multiple sources to provide a useful resource. No detailed comparisons with alternative methods of describing wavefronts have been included nor has any discussion of various methods of wavefront measurement. A comprehensive introduction to these topics is provided by Tyson [37].

References

[1] Thibos, L.N. *J. Refractive Surg*. **2000**, *16*, 363–365.
[2] Advanced Medical Optics/WaveFront Sciences. http://www.wavefrontsciences.com (accessed 2010).
[3] Zernike, F. *Mon. Not. R. Astron. Soc*. **1934,** *94,* 377–384.
[4] Born, M.; Wolf, E. *Principles of Optics*, 7th ed.; Oxford University Press: New York, 1999.
[5] Bhatia, A.B.; Wolf, E. *Proc. Cambridge Phil. Soc*. **1954,** *50,* 40–48.
[6] Mahajan, V.N. Orthonormal Polynomials in Wavefront Analysis. In *Handbook of Optics*, 3rd ed.; McGraw-Hill: New York, 2010; Vol 2, Part 3, Chapter 11.
[7] Nijboer, B.R.A. *Physica* **1947,** *13,* 605–620.
[8] Mahajan, V.N. *Optical Imaging and Aberrations, Part II: Wave Diffraction Optics*; SPIE Press: Bellingham, WA, 2004.
[9] Noll, R.J. *J. Opt. Soc. Am*. **1976,** *66,* 207–211.
[10] Wyant, J. Basic Wavefront Aberration Theory for Optical Metrology. *Applied Optics and Optical Engineering*; Academic Press: New York, 1992; Vol. XI.
[11] Goodwin, E.P.; Wyant, J.C. *Field Guide to Interferometric Optical Testing*; SPIE Press: Bellingham, WA, 2006.
[12] Smolek, M. *Invest. Ophthalmol Visual Sci*. **2003,** *44,* 4676–4681.
[13] Carpio, M.; Malacara, D. *Opt. Commun*. **1994,** *110,* 514–516.
[14] Thibos, L.N.; Applegate, R.A.; Schwiegerling, J.T.; Webb, R.; VSIA Standards Taskforce members. Standards for Reporting the Optical Aberration of Eyes. In *Vision Science and its Applications, TOPS Volume #35*; Lakshminarayanan, V., Ed.; Optical Society of America: Washington DC, 2000; pp 232–245.
[15] Campbell, C.E. *Optom. Vision Sci*. **2003,** *80,* 79–83.
[16] Abramowitz, M.; Stegun, I.A. *Handbook of Mathematical Functions*; Dover: New York, 1972.
[17] Kinter, E. *Opt. Acta* **1976,** *23,* 499–500.
[18] Forbes, G.W. *Opt. Express* **2010,** *18,* 13851–13862.
[19] Malacara, D. *Optical Shop Testing*, 2nd ed.; Wiley, New York, 1992; pp 455–499.
[20] Tyson, R.K. *Opt. Lett*. **1982,** *7,* 262–264.
[21] Conforti, G. *Opt. Lett*. **1983,** *8,* 407–408.
[22] Goldberg, K.A.; Geary, K. *J. Opt. Soc. Am. A* **2001,** *18,* 2146–2152.
[23] Schwiegerling, J. *J. Opt. Soc. Am. A* **2002,** *19,* 1937–1945.
[24] Dai, G. *J. Opt. Soc. Am. A* **2006,** *23,* 539–543.
[25] Campbell, C.E. *J. Opt. Soc. Am. A* **2003,** *20,* 209–217.
[26] Bara, S.; Arines, J.; Ares, J.; Prado, P. *J. Opt. Soc. Am. A* **2006,** *23,* 2061–2066.
[27] Lundstrom, L.; Unsbo, P. *J. Opt. Soc. Am. A* **2007,** *24,* 569–577.
[28] Atchison, D.A.; Scott, D.H. *J. Opt. Soc. Am. A* **2002,** *19,* 2180–2184.
[29] Shen, J.; Thibos, L. *Clin. Exp. Optom*. **2009,** *92,* 212–222.
[30] Prata, A.; Rusch, W.V.T. *Appl. Opt*. **1989,** *28,* 749–754.
[31] Dai, G. *Opt. Lett*. **2006,** *31,* 501–503.
[32] Janssen, A.; Dirksen, P. *J. Eur. Opt. Soc*. **2007,** *2,* 07012.
[33] Dai, G. *J. Refractive Surg*. **2006,** *22,* 943–948.
[34] Yoon, G.; Pantanelli, S.; MacRae, S. *J. Refractive Surg*. **2008,** *24,* 582–590.
[35] Mahajan, V. *J. Opt. Soc. Am*. **1981,** *71,* 75–85.
[36] Upton, R.; Ellerbroek, B. *Opt. Lett*. **2004,** *29,* 2840–2842.
[37] Tyson, R. *Principles of Adaptive Optics*, 3rd ed.; CRC Press: New York, 2010.
[38] Wyant, J.C. Zernike Polynomials for the Web; http://www.optics.arizona.edu/jcwyant/zernikes (accessed 2010).

Appendix 1. Mathematica code

1. Code to generate table of Zernike polynomials (note that the indexing scheme is slightly different – the TableForm command, shown below, in either polar or Cartesian coordinates shows the indexing scheme) [37]

```
nDegree = 6;

i = 0;
Do[If[m == 0, {i = i + 1, temp[i] = {i - 1, n, m, r[n, m, ρ]}},
            {i = i + 1, temp[i] = {i - 1, n, m, Factor[rcos[n, m, ρ]]},
    i = i + 1, temp[i] = {i - 1, n, m, Factor[rsin[n, m, ρ]]}}], {n, 0, nDegree}, {m, n, 0, -1}];

zernikePolarList = Array[temp, i];
Clear[temp];
Do[zernikePolar[i - 1] = zernikePolarList[[i, 4]], {i, 1, Length[zernikePolarList]}];

zernikeXyList = Map[TrigExpand, zernikePolarList] /. {ρ → Sqrt[x^2 + y^2], Cos[θ] → x/Sqrt[x^2 + y^2], Sin[θ] → y/Sqrt[x^2 + y^2]};
Do[zernikeXy[i - 1] = zernikeXyList[[i, 4]], {i, 1, Length[zernikeXyList]}]
```

(a) For table in polar coordinates:

```
TableForm[zernikePolarList, TableHeadings -> {{}, {"#", "n", "m", "Polynomial"}}]
```

(b) For table in Cartesian coordinates:

```
TableForm[zernikeXyList, TableHeadings -> {{}, {"#", "n", "m", "Polynomial"}}]
```

2. For a cylindrical plot:

```
zernikeNumber = 8;

temp = zernikePolar[zernikeNumber];
SurfaceOfRevolution[temp, {ρ, 0, 1}, PlotPoints → 40, BoxRatios → {1, 1, 0.5},
    LightSources -> {{{1., 0., 1.}, RGBColor[1, 0, 0]},
    {{1., 1., 1.}, RGBColor[.5, 1, 0]}, {{0., 1., 1.}, RGBColor[1, 0, 0]},
            {{-1., 0., -1.}, RGBColor[1, 0, 0]}, {{-1., -1., -1.}, RGBColor[.5, 1, 0]},
    {{0., -1., -1.}, RGBColor[1, 0, 0]}}];
```

3. For wavefront aberrations:

```
thirdOrderAberration = {{"piston", w00}, {"tilt", w11 ρ Cos[θ - αTilt]}, {"focus", w20 ρ^2},
   {"astigmatism", w22 ρ^2 Cos[θ - αAst]^2}, {"coma", w31 ρ^3 Cos[θ - αComa]}, {"spherical", w40 ρ^4}};

TableForm[thirdOrderAberration]
```

piston	w_0
tilt	$\rho \cos[\theta - \alpha_{Tilt}]\, w_{11}$
focus	$\rho^2 w_{20}$
astigmatism	$\rho^2 \cos[\theta - \alpha_{Ast}]^2 w_{22}$
coma	$\rho^3 \cos[\theta - \alpha_{Coma}]\, w_{31}$
spherical	$\rho^4 w_{40}$

```
zernikeCoefficient = {z0, z1, z2, z3, z4, z5, z6, z7, z8};
wavefrontAberrationList = Table[zernikeCoefficient zernikePolarList[[Range[1, 9], 4]]];

wavefrontAberrationLabels = {"piston", "x-tilt", "y-tilt", "focus", "astigmatism at 0 degrees & focus",
   "astigmatism at 45 degrees & focus", "coma and x-tilt", "coma and y-tilt", "spherical & focus"};
```

```
Do[
 {tableData[i, 1] = wavefrontAberrationLabels[[i]], tableData[i, 2] = wavefrontAberrationList[[i]]}, {i, 1, 9}]

TableForm[Array[tableData, {9, 2}], TableHeadings → {{}, {"Aberration", "Zernike Term"}}]
wavefrontAberration = Collect[Sum[wavefrontAberrationList[[i]], {i, 9}], ρ]
tilt = Collect[Select[wavefrontAberration, MemberQ[#, ρ ] &], {ρ, Cos[θ], Sin[θ]}];
focusPlusAstigmatism = Select[wavefrontAberration, MemberQ[#, ρ^2 ] &];
coma = Select[wavefrontAberration, MemberQ[#, ρ^3 ] &];
spherical = Select[wavefrontAberration, MemberQ[#, ρ^4 ] &];
tilt = tilt /. a_ Cos[θ_] + b_ Sin[θ] → √a^2 + b^2 Cos[θ - ArcTan[a, b]]
```

4. For concentric scaling:
From:
http://demonstrations.wolfram.com/ZernikeCoefficientsForConcentricCircularScaledPupils/

```
b[order_, np_, m_, ϵ_] :=
Module[{n, coeff},
 coeff =
  Sum[a_{n,m} * √(n + 1) * √(np + 1) *
    ((-1)^((n-2 m+np)/2) * ϵ^np Gamma[1/2 (2 + n + np)] Hypergeometric2F1Regularized[1/2 (-n + np), 1/2 (2 + n + np), 2 + np, ϵ^2])/
     (Gamma[1/2 (2 + n - np)]), {n, np, order, 2}]]


r2c[e_] := FullSimplify[Chop[TrigExpand[e]] /. {Sin[θ] ↦ y/ρ, Cos[θ] ↦ x/ρ} /. ρ^n_ ↦ (x^2 + y^2)^(n/2)];

zPlot[e_, ϵ_] :=
 With[{f = r2c[e]}, ContourPlot[f, {x, -1, 1}, {y, -1, 1},
   RegionFunction → Function[{x, y, z}, 0 ≤ x^2 + y^2 ≤ ϵ], Mesh → False, ImageSize → {180, 180},
   BoundaryStyle → Directive[White, Thick]]]

Zernike[n_, m_, ρ_, θ_] := Sqrt[n + 1] * ZernikeR[n, Abs[m], ρ] *
  Which[m == 0, 1, m > 0, Sqrt[2] * Cos[m * θ], m < 0, (-Sqrt[2]) * Sin[m * θ]];

Zernike[n_, m_, ρ_ /; ρ > 1, θ_] := 0

(*unscaled=Flatten[Table[a_{i,j}→ RandomInteger[{-2,2}],{i,0,order},{j,-i,i,2}]];*)

unscaled = {a_{0,0} → -2, a_{1,-1} → 1, a_{1,1} → 1, a_{2,-2} → -2, a_{2,0} → 1, a_{2,2} → 1, a_{3,-3} → 0, a_{3,-1} → 2, a_{3,1} → 1,
   a_{3,3} → -1, a_{4,-4} → -1, a_{4,-2} → -2, a_{4,0} → 0, a_{4,2} → 1, a_{4,4} → -2, a_{5,-5} → -1, a_{5,-3} → -2, a_{5,-1} → 2, a_{5,1} → -1,
   a_{5,3} → 2, a_{5,5} → -2, a_{6,-6} → -1, a_{6,-4} → 2, a_{6,-2} → 0, a_{6,0} → 2, a_{6,2} → 1, a_{6,4} → -2, a_{6,6} → -1};
f[order_, ratio_] := Module[{i, j, n, W, S, Z},
 scaled =
  Flatten[
   Table[
    b_{i,j} →
     Sum[a_{n,j} * √(n + 1) * √(i + 1) *
       ((-1)^((n-2 j+i)/2) * ratio^i Gamma[1/2 (2 + n + i)] Hypergeometric2F1Regularized[1/2 (-n + i), 1/2 (2 + n + i),
           2 + i, ratio^2])/ (Gamma[1/2 (2 + n - i)]), {n, i, order, 2}], {i, 0, order}, {j, -i, i, 2}]];
 Z = Sum_{i=0}^{order} Sum[a_{i,j} * Zernike[i, j, ρ, θ], {j, -i, i, 2}];
 S = Chop[Sum_{i=0}^{order} Sum[b_{i,j} * Zernike[i, j, ρ, θ] , {j, -i, i, 2}]];
 S = S /. scaled;
 S = S /. unscaled;
 W = Z /. unscaled;
 {W, S}]
```

```
Manipulate[
 Column[{
   W = f[order, r];
   GraphicsRow[{Show[zPlot[W[[1]], 1], Graphics[{White, Thick, Circle[{0, 0}, r]}],
      PlotLabel → "Unit Pupil", LabelStyle → Directive[Bold, Black]],
     Show[zPlot[W[[2]], 1], PlotLabel → "Scaled Pupil ϵ= " <> ToString[r],
      LabelStyle → Directive[Bold, Black]]}],
   Pane[
    Text@TraditionalForm@If[numerico == "numeric",
      Style[
       Table[{b_{np,m}, "=", FullSimplify[Collect[Expand[b[order, np, m, r]], √__ a__],
           (np - m) / 2 ∈ Integers, ComplexityFunction → LeafCount]}, {np, 0, order}] // TableForm, Medium],

      Style[
       Table[{b_{np,m}, "=", FullSimplify[Collect[Expand[b[order, np, m, ϵ]], √__ a__],
           (np - m) / 2 ∈ Integers, ComplexityFunction → LeafCount]}, {np, 0, order}] // TableForm, Medium]],
    ImageSize → {420, 125}]}, Center],
 {{order, 2, "maximum order k"}, Range[0, 6] , ControlType → SetterBar},
 {{r, 0.8, "pupil ratio ϵ"}, 0.001, 1, 0.001, Appearance → "Labeled",
  Enabled → Dynamic[numerico === "numeric"]} ,
 {{numerico, "numeric", "values"}, {"numeric", "analytic"}},
 SaveDefinitions → True, ControlPlacement → Top, ContinuousAction → False, TrackedSymbols → True]
```

5. For conversion of Zernike coefficients for scaled, translated or rotated pupils [27] corresponding to the coordinate system depicted in Figure 5:

```
thetaT = ArcTan[ty/tx];
dia1 = First[C1];
C1 = Rest[C1];
etaS = dia2/dia1;
etaT = 2*Sqrt[tx^2 + ty^2]/dia1;
thetaR = thetaR*Pi/180;
jnm = Length[C1] - 1;
nmax = Ceiling[(-3 + Sqrt[9 + 8*jnm])/2];
jmax = nmax*(nmax + 3)/2;
C1 = Table[If[i < (jnm + 2), C1[[i]], 0. ], {i, 1, jmax + 1}];
P = Table[0, {i, 1, jmax + 1}, {j, 1, jmax + 1}];
nN = Table[0, {i, 1, jmax + 1}, {j, 1, jmax + 1}];
R = Table[0, {i, 1, jmax + 1}, {j, 1, jmax + 1}];
CC1 = Table[0, {i, 1, jmax + 1}];
counter = 1;
For[m = -nmax, m <= nmax, m++,
    For[n = Abs[m], n <= nmax, n = n + 2,
        jnm = (m + n*(n + 2))/2;
        P[[counter, jnm + 1]] = 1;
        nN[[counter, counter]] = Sqrt[n + 1];
        For[s = 0, s <= (n - Abs[m])/2, s++, R[[
      counter - s, counter]] = ((-1)^s)*Factorial[n - s]/(
    Factorial[s]*Factorial[(n + m)/2 - s]*Factorial[(n - m)/2 - s]); ];
        If[m < 0, CC1[[jnm + 1]] = (C1[[(-m + n*(n +
              2))/2 + 1]] + I*C1[[jnm + 1]])/Sqrt[2], If[m == 0, CC1[[
          jnm + 1]] = C1[[jnm +
            1]], CC1[[jnm + 1]] = (C1[[jnm + 1]] - I*C1[[(-m + n*(n + 2))/
            2 + 1]])/Sqrt[2]]] ;
        counter = counter + 1;
        ];];
ETA = {};
```

```
For[m = -nmax, m < (nmax + 1), m++, For[n = Abs[m], n < (nmax + 1), n = n + 2,
         transform = Table[0, {i, 1, jmax + 1}];
        For[p = 0, p < (((n + m)/2) + 1), p++, For[q = 0, q < (((
    n - m)/2) + 1), q++, nnew = n - p - q; mnew = m - p + q;
              jnm = (mnew + nnew*(nnew + 2))/2;
              transform[[Floor[jnm + 1]]] = transform[[Floor[
        jnm + 1]]] + Binomial[(
          n + m)/2, p]*Binomial[(n - m)/2, q]*etaS^(n - p - q)*etaT^(p + q)*
        Exp[I*((p - q)*(thetaT - thetaR) + m*thetaR)];];];
        ETA = Append[ETA, P.transform];];];
ETA = Transpose[ETA];
CC2 = Inverse[P].Inverse[nN].Inverse[R].ETA.R.nN.P.CC1;
C2 = Table[0, {i, 1, jmax + 1}];
For[m = -nmax, m ≤ nmax, m++, For[n = Abs[m], n ≤ nmax,
              n = n + 2, jnm = (m + n*(n + 2))/2;
        If[m < 0, C2[[jnm + 1]] = N[Im[CC2[[jnm + 1]] -
              CC2[[(-m + n*(n + 2))/2 + 1]]]/Sqrt[2]], If[m == 0,
          C2[[jnm + 1]] = N[Re[CC2[[jnm + 1]]]], C2[[jnm + 1]] = N[
              Re[CC2[[jnm + 1]] + CC2[[(-m + n*(n + 2))/2 +
            1]]]/Sqrt[2]]]];];

C2 = Prepend[C2, N[dia2]];
Print[C2];
```

6. For interactive display and plotting including annular pupils:
http://demonstrations.wolfram.com/ZernikePolynomialsAndOpticalAberration/